The Climate Effects of High Latitude Volcanic Eruptions: The Role of the Time of Year

Ben Kravitz and Alan Robock

Department of Environmental Sciences, Rutgers University, New Brunswick, New Jersey

Submitted to *Journal of Geophysical Research*

May, 2010

Ben Kravitz, Department of Environmental Sciences, Rutgers University, 14 College Farm Road, New Brunswick, NJ 08901, USA. (benkravitz@envsci.rutgers.edu) **(Corresponding Author)**

Alan Robock, Department of Environmental Sciences, Rutgers University, 14 College Farm Road, New Brunswick, NJ 08901, USA. (robock@envsci.rutgers.edu)

Abstract

We test how the time of year of a large Arctic volcanic eruption determines the climate impacts by conducting simulations with a general circulation model of Earth's climate. For an injection of 5 Tg of SO_2 into the lower stratosphere, an eruption in June will cause detectable climate effects, whereas an eruption in August will cause negligible effects. The ocean retains memory of the climate effects from a 5 Tg June eruption. In both cases, the sulfate aerosols that form do not persist into the following spring due to large-scale deposition. Our simulations of the June eruption have many similar features to previous simulations of the eruption of Katmai in 1912, including some amount of cooling over Northern Hemisphere continents in the summer of the eruption, which is an expected climate response to large eruptions. Previous Katmai simulations show a stronger climate response, which we attribute to differences in choices of climate model parameters.

1. Introduction

The past year has seen significant volcanic activity, most notably the two large eruptions of Kasatochi Volcano (52.1°N, 175.3°W) on August 8, 2008 and Sarychev Volcano (48.09°N, 153.20°E) on June 12, 2009. Each injected between 1 and 2 Tg of SO_2 into the lower stratosphere [*Carn*, 2008; *Corradini et al*., 2010; *Haywood et al*., 2010], making them the largest volcanic eruptions since Mount Pinatubo and Mount Hudson in 1991 [*Carn and Krueger*, 2004].

Sulfate aerosols, formed from the oxidation of SO_2, have a long atmospheric lifetime in the stratosphere of 1-3 years [*Budyko*, 1977; *Stenchikov et al*., 1998]. They efficiently backscatter shortwave radiation, effectively increasing the planetary albedo for the lifetime of the aerosols [*Robock*, 2000]. This results in the primary climate effect of large volcanic eruptions, which is cooling of the surface and the troposphere during the boreal summer. Since sulfate aerosols are not perfect scatterers, the stratosphere warms after a large eruption [*Stenchikov et al.*, 1998], which can result in dynamical effects due to the alteration of the thermal profile of the lower and middle atmosphere. For large tropical eruptions, these effects include warming over the Northern Hemisphere continents during the boreal winter and a positive mode of the Arctic Oscillation [*Robock*, 2003; *Stenchikov et al*., 2002, 2004].

Additionally, large volcanic eruptions cause significant perturbations to the hydrological cycle [*Trenberth and Dai*, 2007], which is magnified under high latitude eruptions. This mostly takes effect as a reduction of the Indian-African-Asian monsoon, due to differentially reduced solar flux over the Indian Ocean and the large land masses of Asia and Africa [*Kravitz et al.*, 2010]. This effect is magnified for high latitude eruptions, and evidence of it has been seen in past proxy records and climate simulations of the eruptions of Laki in 1783-1784 at 68°N

[*Thordarson and Self*, 2003; *Oman et al.*, 2006a] and Katmai on June 6, 1912 at 58°N [*Oman et al.*, 2005, 2006b].

Despite their large amount of atmospheric SO_2 loading, the eruption of Kasatochi had little to no climate response [*Kravitz et al.*, 2010], and we expect the same findings for Sarychev. We postulate this is due to an insufficient amount of SO_2, despite being such relatively large eruptions. *Kravitz et al.* [2010] performed additional climate model simulations involving a 5 Tg eruption on August 8, but still no climate effects were observed. This is puzzling, since 5 Tg of SO_2 is known to be sufficient to cause climate perturbations, specifically the eruption of Katmai on June 6, 1912 [*Oman et al.*, 2005]. Thus we conjecture that the time of year of a large eruption plays a critical role in determining whether it will have a climate impact.

2. Experiment

We simulated the climate response to high latitude volcanic eruptions with ModelE, a coupled atmosphere-ocean general circulation model developed by the National Aeronautics and Space Administration Goddard Institute for Space Studies [*Schmidt et al.*, 2006]. We used the stratospheric version with 4° latitude by 5° longitude horizontal resolution and 23 vertical levels up to 80 km. It is fully coupled to a 4° latitude by 5° longitude dynamic ocean with 13 vertical levels [*Russell et al.*, 1995]. The aerosol module [*Koch et al.*, 2006] accounts for SO_2 conversion to sulfate aerosols, hydration of the aerosols from a specified dry radius of 0.25 μm, based on formulas by *Tang* [1996], and transport and removal of the aerosols. Radiative forcing (called "adjusted forcing" in *IPCC* [2001] and *Hansen et al.* [2005]) is fully interactive with the atmospheric circulation. For further details, see *Kravitz et al.* [2010], which uses the same model setup.

Our control ensemble was a 20-member ensemble of 4-year runs (2007-2010), during which greenhouse gas concentrations increased according to the Intergovernmental Panel on Climate Change's A1B scenario [*IPCC*, 2007]. When testing the model after this period by conducting simulations of constant 2007 greenhouse gas and aerosol concentrations, no temperature trend was detected for the period 2007-2010, which is the period over which our simulations have been conducted.

To examine the effects of the volcanic eruptions, we used six 20-member ensembles of 4-year simulations covering the same time period. In these simulations, greenhouse gas concentrations increased in the same manner as in the control runs. We also injected SO_2 into the grid box centered at 52°N, 172.5°W, distributed equally in the three model layers that cover an altitude of 10-16 km. Three ensembles had an injection on June 12, 2008, and three had an injection on August 8, 2008, in the amounts of 1.5 Tg, 3 Tg, and 5 Tg of SO_2. The 1.5 Tg injections are meant to simulate the eruptions of Sarychev and Kasatochi. The 3 Tg and 5 Tg injections were included as part of a sensitivity study, although the 5 Tg June eruption is comparable to the eruption of Katmai on June 6, 1912. In section 5, we perform such a comparison between our simulations of a June eruption and a set of simulations of Katmai which were performed for *Oman et al.* [2005].

For their simulations of the 1912 eruption of Katmai, *Oman et al.* [2005] correlated their modeling results with data that showed a climate response to the eruption. This agreement between the model and observations or proxy records has also been verified for the eruptions of Laki in 1783-1784 [*Oman et al.*, 2006a, 2006b] and Pinatubo in 1991 [*Robock et al.*, 2007]. Therefore, we are confident in the model's ability to give us a realistic assessment of large scale climate perturbations from volcanic eruptions.

105

106 **3. The Role of the Time of Year**

107 *Kravitz et al.* [2010] analyzed both the modeled and observed climate impacts of the
108 eruption of Kasatochi and determined such impacts were negligible. Preliminary analysis (not
109 pictured) shows the same results for Sarychev. We conclude that a high latitude volcanic
110 eruption that injects 1.5 Tg of SO_2 into the lower stratosphere is of insufficient magnitude to
111 cause significant climate impacts.

112 To test our hypothesis that the time of year is important in determining whether a high
113 latitude eruption will have climate impacts, we wanted to simulate volcanic eruptions in June and
114 August of a magnitude that is known to cause a detectable climate perturbation in both model
115 studies and observations. Therefore, we chose to simulate a volcanic eruption that injected 5 Tg
116 of SO_2 into the lower stratosphere, as this was the atmospheric loading due to Katmai.

117 Figure 1 shows a comparison of Northern Hemisphere averaged aerosol optical depth
118 (mid-visible, λ=550 nm) and shortwave radiative forcing at the surface due to the sulfate aerosols
119 for all six of the climate model simulation ensembles. As expected, aerosol optical depth and
120 radiative forcing both increase approximately linearly with increased atmospheric loading of
121 SO_2. Also, aerosol optical depth drops to low levels (below 0.01) well before the spring after the
122 eruption. Radiative forcing drops to low levels (smaller in magnitude than –0.25 W m^{-2}) at
123 approximately the same time. Of particular interest in this figure is that the aerosols from the
124 August eruption stay above this threshold (greater in magnitude than –0.25 W m^{-2})
125 approximately one month later than the aerosols in the June eruption. This suggests a stronger
126 rate of deposition in the winter than in the autumn, as well as shows the rate of deposition is
127 proportional to the amount of aerosol in the atmosphere. The June eruptions reach larger peak

radiative forcing than do the August eruptions, which is likely due to the much larger value of insolation affected by the June eruption than the August eruption. The peak values of aerosol optical depth are comparable, regardless of the time of the eruption. All values of aerosol optical depth and radiative forcing return to background levels within a year after the eruptions.

Figures 2 and 3 show the same results in more spatial and temporal detail. We see in Figure 2 that even in the zonal average instead of the Northern Hemisphere average, sulfate aerosol optical depth drops to low levels (below 0.01) by the spring after the eruption, and well before the spring for all but the two 5 Tg eruptions. Aerosol optical depth values reach higher peaks in the June eruptions than the corresponding August eruptions due to lower deposition rates in the summer, allowing aerosols formed in the summer to linger in the atmosphere. Although the bulk of the aerosols stays north of 30°N in latitude, the magnitude of the eruption appears to correlate with the maximum longitudinal extent of the aerosol plume. The 5 Tg eruptions show evidence of a small amount of aerosols reaching into the tropics.

Radiative forcing patterns in Figure 3 closely parallel the patterns of optical depth, with peak negative forcings occurring approximately one month after the eruptions, but the the radiative forcing from the June eruptions is enhanced by the larger amount of insolation available in the late summer. In addition, the June eruptions reach higher magnitude peaks than their corresponding August eruptions, due to lower rates of deposition in the summer. Radiative forcing again drops to low levels (smaller in magnitude than -0.25 W m^{-2}) well before the following spring for all but the two 5 Tg eruptions. As in Figure 2, there is evidence of some amount of aerosol extending well into the tropics, particularly for the larger eruptions in this study. The 5 Tg eruption in June also shows that some of the aerosols persisted through the

150 winter into the following year, showing measurable levels of radiative forcing until one year
151 after the eruption.

152 Figure 4 shows line graphs of Northern Hemisphere averaged surface air temperature
153 anomaly (volcano plus A1B ensemble minus A1B ensemble) and globally averaged precipitation
154 anomaly for all six ensembles. For the 5 Tg eruptions, the June eruption shows a stronger
155 decrease in temperature than the August eruption by nearly a factor of two. Also, even a 3 Tg
156 eruption in June shows more cooling than a 5 Tg eruption in August, strongly suggesting a
157 confirmation of our hypothesis that the time of year of an eruption is critical in estimating
158 climate impact. Moreover, there is very little difference between the climate impact of the 3 Tg
159 and 5 Tg August eruptions, which suggests the August eruptions are too late in the year to cause
160 a climate impact. We do not detect any significant signal in globally averaged precipitation due
161 to any of the eruptions. This is not unreasonable, since not only does precipitation have a large
162 natural variability, but for all simulations, the aerosols formed well after June, missing the
163 chance to mitigate a large amount of summer continental heating. We also analyzed spatial maps
164 of summer precipitation for these eruptions (not pictured) but found no patterns to suggest a
165 reduction in the summer monsoon system.

166 For the calendar year (2009) after the 5 Tg eruption in June, the average Northern
167 Hemisphere surface air temperature is 0.06°C lower than the calendar year before the eruption
168 (2007), or over 20% of the simulated temperature anomaly in September, 2008. A natural
169 explanation for this could be ocean memory of the cooling due to the eruption [*Stenchikov et al.*,
170 2009]. Although the version of the model we used to perform the simulations in this experiment
171 does not provide us with enough information to assess changes in ocean heat content, we can still
172 evaluate some oceanic changes. Figure 6 proceeds with this investigation, showing ocean

potential temperature anomaly for the top eight layers in the model's ocean. The depths of the model's ocean layers are given in Figure 5. In the top five of these layers, we see a sharp, discontinuous cooling immediately after the volcanic eruption. Layers 1 and 2, which constitute the mixed layer at this time of year, show the largest drop. Despite technically being at the top of the thermocline according to *de Boyer Montégut et al.* [2004], one could argue layer 3 is actually part of the mixed layer, due to its precipitous drop in temperature immediately after the volcanic eruption. Layers 4 and 5 also show a sharp drop, although not nearly as strongly as found in layers 1-3 and delayed several months after the drop in the upper layers, suggesting layers 4 and 5 are below the mixed layer. Layers 6 and 7 show a slight warming over the period affected by the volcano, which can possibly represent a change in mixing and ocean dynamics due to the perturbed temperatures. However, we again do not have enough information in our model output to diagnose the cause of this change. Layer 8 shows little variability, suggesting the volcanic signal is not felt in the deep ocean during the time period represented in these simulations. Layers 1 and 2 return to zero anomaly only by the end of the simulation, and layers 3 and 4 still have not recovered to zero anomaly by this time. We expect the recovery of layers below the mixed layer to be slower, since these are much more removed from the atmospheric seasonal cycle than are the surface layers. Although we do not have enough model output to make any conclusions regarding statistical significance of these anomalies, our results suggest the suppression of the average temperature after the eruption could be due to ocean memory of volcanic cooling.

Figure 7 shows the 171 mb height anomalies for the winter following the eruptions for the 5 Tg eruptions on June 12 and August 8. This model layer was chosen because it is in the lower stratosphere, at the center of the range over which the SO_2 was injected. This layer's

196 height shows the degree of stratospheric heating and resulting dynamical effects due to the
197 sulfate aerosols. The June eruption shows a statistically significant pattern of increased height,
198 centered over Hudson Bay and Eastern Europe. This is accompanied by a strong, though not
199 statistically significant, reduction in height centered over Alaska. In contrast, the August
200 eruption shows very few values of statistical significance, although the magnitude of reduced
201 height over Alaska is similar. The June eruption shows a pattern that could be interpreted as a
202 weak mode 3 oscillation, while the August eruption shows no such pattern. In neither case is this
203 pattern indicative of modification of a more well-known large scale pattern such as the Arctic
204 Oscillation or the North Atlantic Oscillation.
205
206 **4. Discussion**
207 To evaluate the statistical significance of the anomalies in Figure 4, we analyzed data
208 provided by the National Climatic Data Center (NCDC) and the University of East Anglia's
209 Climatic Research Unit (CRU). From NCDC, we obtained gridded data at 5° latitude by 5°
210 longitude, created from version 2 of the Global Historical Climatology Network (GHCNv2)
211 [*Free et al.*, 2004; *Peterson and Vose*, 1997; *Peterson et al.*, 1998]. From CRU, we obtained
212 variance adjusted land air temperature anomalies, also gridded at 5° latitude by 5° longitude
213 (CRUTEM3v) [*Brohan et al.*, 2006; *Jones et al.*, 1999; *Rayner et al.*, 2003, 2006].
214 Calculations were performed based on a Student's t test with the number of degrees of
215 freedom equal to the number of years in each of the sources' records, which is 130 for the NCDC
216 GHCNv2 temperature record (1880-2009), 110 for the NCDC GHCNv2 precipitation record
217 (1900-2009), and 160 for the CRUTEM3v temperature record (1850-2009). (We were unable to
218 obtain precipitation data from CRU.) For an anomaly to be statistically significant at the 95%

confidence level, it must be at least 0.21°C different from a 12 month centered running mean (t-6 months to t+5 months) according to GHCNv2 data and at least 0.24°C according to CRUTEM3v data. To be significant at the 90% level, it must be 0.18°C or 0.20°C different from the 12 month running mean, respectively. The difference between the values for the two records is due to the number of degrees of freedom each record has. Precipitation must be 0.23 mm/day different from the 12 month running mean to be significant at the 95% level and 0.19 mm/day to be significant at the 90% level.

For the values reported in Figure 4, only the 5 Tg eruption on June 12 has statistically significant anomalies according to the above criteria. For this ensemble, the September anomaly is 0.21°C lower than the 12-month running mean centered on that month, meaning it is statistically significant at the 90% confidence level according to both sets of data and at the 95% confidence level according to the GHCNv2 data. This is the only point of all ensembles that is statistically significant at the 90% level or better. No precipitation values are statistically significant at either the 90 or 95% confidence levels, and the actual anomaly values are approximately one order of magnitude below the global average values needed to be considered significant.

These results reinforce current knowledge about the climate effects of large volcanic eruptions. Although a 5 Tg eruption in June does have detectable climate effects according to *Oman et al.* [2005], the effects of Katmai were found to be only barely distinguishable from weather noise. Moreover, not only is precipitation highly variable, hampering the ease by which an anomaly can be considered significant, but the aerosols would have completely formed well after June, so the first part of the monsoon, as well as the time period with the greatest amount of insolation, would be largely unaffected.

5. Comparison to Katmai

One addition to this study is a comparison to the effects of the eruption of Katmai (Novarupta) Volcano (58.28°N, 154.96°W) on June 6, 1912, which injected 5 Tg of SO_2 into the lower stratosphere. Katmai was known to have climate effects, including cooling over Northern Hemisphere continents in the summer of the eruption and a weakening of the Indian-African monsoon system, as was evidenced by low river flow in those areas [*Oman et al.*, 2005]. In this section, we compare our results with those of *Oman et al.*, who performed simulations of Katmai with a very similar setup of the same model.

The simulations performed by *Oman et al.* [2005] involved two ensembles. The control ensemble was composed of ten model runs at constant greenhouse gas and aerosol concentrations, and was then time-averaged to produce a 40 member ensemble. The volcano ensemble was an average of 20 runs using the same conditions as the control runs, but involving specified aerosol optical depths from *Ammann et al.* [2003], corrected to have a variable aerosol effective radius, as in *Sato et al.* [1993], which is in good agreement with *Stothers* [1997]. This is in contrast to our simulations, in which sulfate aerosol formation was calculated in the model. We also used a fully dynamic ocean, whereas *Oman et al.* used fixed sea surface temperatures and sea ice conditions prescribed by a 1946-1955 average [*Rayner et al.*, 2003].

Figure 8 shows plots of surface air temperature anomaly due to a 5 Tg eruption on June 12, 2008, compared to the same results for simulations of the eruption of Katmai. We only show plots for surface air temperature, as Figure 4 suggests our plots of precipitation will show no significant results (which indeed they do not; not pictured), and *Oman et al.* [2005] similarly do not include plots of precipitation for their simulations of Katmai. Both sets of simulations show

very similar patterns for the summer of the eruption (JJA), including a general pattern of cooling over the Northern Hemisphere continents, and the winter after the eruption (DJF) in the form of warming over the Northern Hemisphere continents.

However, the patterns that appear in the simulations of Katmai are generally stronger and more pronounced than the anomalies in our simulations. We suggest several reasons for this discrepancy. First, we would not expect the patterns to be identical, since our aerosols are formed by the model and interact with the circulation, whereas the aerosols in the Katmai simulations do not. Our peak values of aerosol optical depth are consistent with those of *Oman et al.* (0.3 in September after the eruption). Moreover, fixed sea surface temperatures would negate the ocean memory effect seen in Figure 6, and using fixed sea surface temperatures can amplify surface air temperature anomalies, offering an additional explanation for the larger anomalies in the Katmai simulations [*Hansen et al.*, 2005]. Additionally, *Oman et al*. performed their statistical tests differently, using a single sample Student's t test based on 40 years of control runs. We used an unpaired two sample Student's t test based on 20 runs each. This difference in calculations appears to have the effect of making more of their results statistically significant than ours, given similar levels of anomaly.

6. Relevance to stratospheric geoengineering

This study is highly relevant to geoengineering with stratospheric sulfate aerosols, as it shows that not only does the amount of injection of sulfate aerosol precursor into the stratosphere significantly impact the climate effects, but also the timing of the injection is crucial. Past modeling studies have failed to capture this importance, especially in studies of Arctic injection. *Robock et al.* [2008] performed an experiment of geoengineering with stratospheric sulfate

aerosols in the Arctic, but their simulations involved year-round injection of SO_2. Our results suggest autumn injections are not necessary, since their climate effects would be negligible. Moreover, winter injections in the Arctic are superfluous, since the lack of sunlight in high latitudes in the winter precludes any potential radiative effects from the aerosols.

A natural consequence of these results would be to perform model simulations of Arctic geoengineering in the boreal spring, ceasing injections of SO_2 for the rest of the year. Not only would this be less invasive than year-round injections, but it would also take advantage of our findings. We caution any modeling groups conducting such simulations to ensure the amount of SO_2 they inject is of sufficient quantity to cause measurable surface cooling. However, we believe our findings should strongly discourage real-world testing of Arctic geoengineering, regardless of the time of year. *Oman et al.* [2005] and *Robock et al.* [2008] clearly show that any forcing from the aerosols that reduced surface temperatures would also weaken the monsoon system as a dynamical consequence. Moreover, to observe the results at a satisfactory level of statistical significance, geoengineering would need to be conducted for a long period of time [*Robock et al.*, 2010]. Indeed, our simulations were conducted with 20 ensemble members, and our results were barely statistically significant, indicating that observing test results of geoengineering at the same level of certainty would require deployment for at least 20 years, which is quite a long period of time over which side effects will be felt.

Our findings regarding ocean memory are also likely to be pertinent for geoengineering simulations. We suspect the cooling due to geoengineering would be enhanced by this oceanic effect, especially if done every year. However, we are unable to quantify this effect without further investigation.

7. Conclusions

Based on our climate modeling study, the time of year of a volcanic eruption is important in determining the resulting climate effects, provided the eruption is large enough. For a June eruption, both we and *Oman et al.* [2005] have shown that a 5 Tg eruption is sufficient to cause detectable climate impacts. For an August eruption, 5 Tg is still insufficient to cause an impact. Indeed, we show that the time of year of an eruption is of equal, if not greater, importance than the size of the eruption.

In line with *Stenchikov et al.* [2009], we further conclude the ocean has memory of the cooling an eruption causes, which can serve to modulate changes in climate. However, the runs we have completed are not long enough to fully assess the impacts of the ocean on the climate system. We stress that simulations of large eruptions need to include a complex ocean to capture these potentially important effects.

Future work on this topic could include testing an even earlier high latitude eruption, perhaps in April or even before. We could also attempt to determine how large an August eruption must be to have climate impacts. Additionally, we could perform a similar suite of experiments, but for tropical injections, to determine the relationship between climate effects and latitude. This last idea would also affect more surface area of the planet, making easier any further analysis of ocean memory.

Acknowledgments. Model development and computer time at Goddard Institute for Space Studies are supported by National Aeronautics and Space Administration climate modeling grants. This work is supported by NSF grant ATM-0730452.

References

Ammann, C. M., G. A. Meehl, W. M. Washington, and C. S. Zender (2003), A monthly and latitudinally varying volcanic forcing dataset in simulations of 20th century climate, *Geophys. Res. Lett.*, *30*(12), 1657-1660, doi:10.1029/2003GL016875.

Brohan, P. J. J. Kennedy, I. Harris, S. F. B. Tett, and P. D. Jones (2006), Uncertainty estimates in regional and global observed temperature changes: A new dataset from 1850, *J. Geophys. Res.*, *111*, D12106, doi:10.1029/2005JD006548.

Budyko, M. I. (1977), *Climatic Changes* (American Geophysical Union, Washington, DC), 261 pp.

Carn, S. (2008), Sulfur dioxide cloud from Aleutians' Kasatochi volcano, NASA Earth Observatory, http://earthobservatory.nasa.gov/images/imagerecords/8000/8998/kasatochi_OMI_2008aug11_lrg.jpg.

Carn, S. and A. Krueger (2004), TOMS Volcanic Emissions Group, http://toms.umbc.edu/Images/Mainpage/toms_so2chart_color.jpg.

Corradini, S., L. Merucci, A. J. Prata, and A. Piscini (2010), Volcanic ash and SO_2 in the Kasatochi and Okmok eruptions: Retrievals from different IR satellite sensors, *J. Geophys. Res.*, special issue, submitted.

de Boyer Montégut, C., G. Madec, A. S. Fischer, A. Lazar, and D. Iudicone (2004), Mixed layer depth over the global ocean: An examination of profile data and a profile-based climatology, *J. Geophys. Res.*, *109*, C12003, doi:10.1029/2004JC002378.

Free, M., J. K. Angell, I. Durre, J. Lanzante, T. C. Peterson, and D. J. Seidel (2004), Using first differences to reduce inhomogeneity in radiosonde temperature datasets, *J. Climate, 21*, 4171-4179.

Hansen, J., et al. (2005), Efficacy of climate forcings, *J. Geophys. Res.*, *110*, D18104, doi:10.1029/2005JD005776.

Haywood, J., et al. (2010), Observations and simulations of the eruption of the Sarychev volcano using HadGEM2, in preparation.

IPCC (2001), *Climate Change 2001: The Scientific Basis*. Contribution of Working Group I to 1006 the Third Assessment Report of the Intergovernmental Panel on Climate Change, Houghton, J. T., Y. Ding, D. J. Griggs, M. Noguer, P. J. van der Linden, X. Dai, K. Maskell, and C.A. Johnson, Eds., (Cambridge University Press, Cambridge, United Kingdom and New York, NY, USA), 881 pp.

IPCC (2007), *Climate Change 2007: The Physical Science Basis. Contribution of Working Group I to the Fourth Assessment Report of the Intergovernmental Panel on Climate Change*, S. Solomon, D. Qin, M. Manning, Z. Chen, M. Marquis, K. B. Averyt, M. Tignor and H. L. Miller, Eds., (Cambridge University Press, Cambridge, United Kingdom and New York, NY, USA), 996 pp.

Jones, P. D., M. New, D. E. Parker, S. Martin, and I. G. Rigor (1999), Surface air tmperature and its variations over the last 150 years, *Rev. Geophys.*, *37*, 173-199.

Koch, D., G. A. Schmidt, and C. V. Field (2006), Sulfur, sea salt, and radionuclide aerosols in GISS ModelE, *J. Geophys. Res.*, *111*, D06206, doi:10.1029/2004JD005550.

Kravitz, B., A. Robock, and A. Bourassa (2010), Negligible climatic effects from the 2008 Okmok and Kasatochi volcanic eruptions, *J. Geophys. Res.*, doi:10.1029/2009JD013292, in press.

Oman, L., A. Robock, G. L. Stenchikov, G. A. Schmidt, and R. Ruedy (2005), Climatic response to high-latitude volcanic eruptions, *J. Geophys. Res.*, *110*, D13103, doi:10.1029/2004JD005487.

Oman, L., A. Robock, G. L. Stenchikov, T. Thordarson, D. Koch, D. T. Shindell, and C. Gao (2006a), Modeling the distribution of the volcanic aerosol cloud from the 1783-1784 Laki eruption, *J. Geophys. Res.*, *111*, D12209, doi:10.1029/2005JD006899.

Oman, L., A. Robock, G. L. Stenchikov, and T. Thordarson (2006b), High-latitude eruptions cast shadow over the African monsoon and the flow of the Nile, *Geophys. Res. Lett.*, *33*, L18711, doi:10.1029/2006GL027665.

Peterson, T. C. and R. S. Vose (1997), An overview of the Global Historical Climatology Network temperature data base, *Bull. Amer. Met. Soc.*, *78*, 2837-2849.

Peterson, T. C., T. R. Karl, P. F. Jamason, R. Knight, and D. R. Easterling (1998), The first difference method: Maximizing station density for the calculation of long-term global temperature change, *J. Geophys. Res. Atm.*, *103*(D20), 25967-25974.

Rayner, N. A., D. E. Parker, E. B. Horton, C. K. Folland, L. V. Alexander, D. P. Rowell, E. C. Kent, and A. Kaplan (2003), Globally complete analyses of sea surface temperature, sea ice, and night marine air temperature, 1871-2000, *J. Geophys. Res.*, *108*, 4407-4435, doi:10.1029/2002JD002670.

Rayner, N. A., P. Brohan, D. E. Parker, C. K. Folland, J. J. Kennedy, M. Vanicek, T. Ansell, and S. F. B. Tett (2006), Improved analyses of changes and uncertainties in marine temperature measured in situ since the mid-nineteenth century: The HadSST2 dataset, *J. Climate*, *19*, 446-469.

Robock, A. (2000), Volcanic eruptions and climate, *Rev. Geophys.*, *38*, 191-219.

401 Robock, A. (2003), Volcanoes: Role in climate, in *Encyclopedia of Atmospheric Sciences*, J.
402 Holton, J. A. Curry, and J. Pyle, Eds., (Academic Press, London), 2494-2500,
403 10.1006/rwas.2002.0169.
404 Robock, A. T. Adams, M. Moore, L. Oman, and G. Stenchikov (2007), Southern hemisphere
405 atmospheric circulation effects of the 1991 Mount Pinatubo eruption, *Geophys. Res. Lett.*, *34*,
406 L23710, doi:10.1029/2007GL031403.
407 Robock, A., L. Oman, and G. Stenchikov (2008), Regional climate responses to geoengineering
408 with tropical and Arctic SO_2 injections, *J. Geophys. Res.*, *113*, D16101, doi:10.1029/
409 2008JD010050.
410 Robock, A., M. Bunzl, B. Kravitz, and G. Stenchikov (2010), A test for geoengineering?,
411 *Science*, *327*(5965), 530-531, doi:10.1126/science.1186237.
412 Russell, G. L., J. R. Miller, and D. Rind (1995), A coupled atmosphere-ocean model for transient
413 climate change, *Atmos.-Ocean*, *33*, 683-730.
414 Sato, M., J. E. Hansen, M. P. McCormick, and J. B. Pollack (1993), Stratospheric aerosol optical
415 depths, 1850-1990, *J. Geophys. Res.*, *98*, 22987-22994.
416 Schmidt, G. A., et al. (2006), Present day atmospheric simulations using GISS ModelE:
417 Comparison to in situ, satellite and reanalysis data, *J. Climate*, *19*, 153-192.
418 Stenchikov, G. L., I. Kirchner, A. Robock, H.-F. Graf, J. C. Antuña, R. G. Grainger, A. Lambert,
419 and L. Thomason (1998), Radiative forcing from the 1991 Mount Pinatubo volcanic
420 eruption, *J. Geophys. Res.*, *103*, 13837-13857, doi:10.1029/98JD00693.
421 Stenchikov, G., A. Robock, V. Ramaswamy, M. D. Schwarzkopf, K. Hamilton, and S.
422 Ramachandran (2002), Arctic Oscillation response to the 1991 Mount Pinatubo eruption:

Effects of volcanic aerosols and ozone depletion. *J. Geophys. Res.*, *107(D24)*, 4803, doi:10.1029/2002JD002090.

Stenchikov, G., K. Hamilton, A. Robock, V. Ramaswamy, and M. D. Schwarzkopf (2004), Arctic Oscillation response to the 1991 Pinatubo eruption in the SKYHI GCM with a realistic Quasi-Biennial Oscillation. *J. Geophys. Res.*, *109*, D03112, doi:10.1029/2003JD003699.

Stenchikov, G., T. L. Delworth, V. Ramaswamy, R. J. Stouffer, A. Wittenberg, and F. Zeng (2009), Volcanic signals in oceans, *J. Geophys. Res.*, *114*, D16104, doi:10.1029/2008JD011673.

Stewart, R. H. (2007), Introduction to physical oceanography, 345 pp.

Stothers, R. B. (1997), Stratospheric aerosol clouds due to very large volcanic eruptions of the early twentieth century: Effective particle sizes and conversion from pyrheliometric to visual optical depth, *J. Geophys. Res.*, *102*(D5), 6143-6151.

Tang, I. N. (1996), Chemical and size effects of hygroscopic aerosols on light scattering coefficients, *J. Geophys. Res.*, *101*, D14, 19245-19250.

Thordarson, T. and S. Self (2003), Atmospheric and environmental effects of the 1783-1784 Laki eruption: A review and reassessment, *J. Geophys. Res.*, *1108*(D1), 4011, doi:10.1029/2001JD002042.

Trenberth, K. E., and A. Dai (2007), Effects of Mount Pinatubo volcanic eruption on the hydrological cycle as an analog of geoengineering, *Geophys. Res. Lett.*, *34*, L15702, doi:10.1029/2007GL030524.

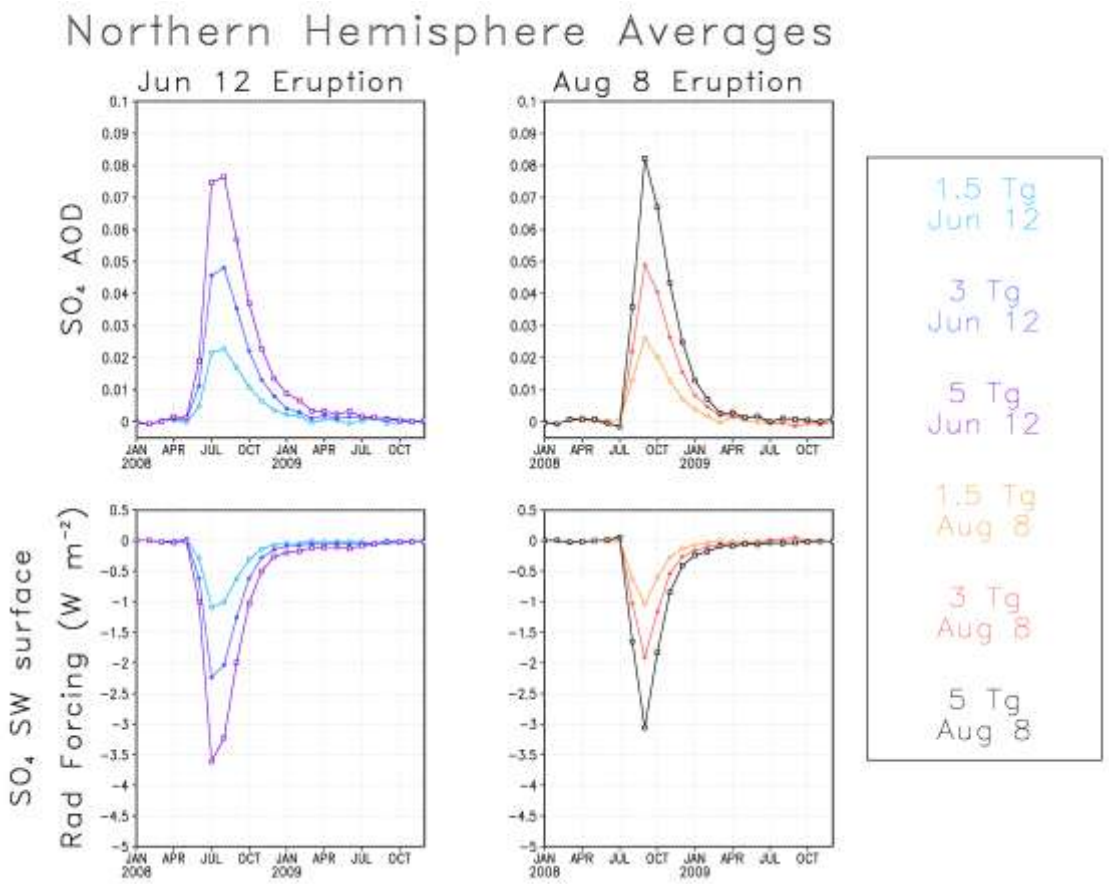

443

444 **Figure 1.** Northern Hemisphere averages for all six ensembles of sulfate aerosol optical depth and shortwave radiative forcing at the
445 surface due to sulfate aerosols. All ensembles pictured are averages of 20 model runs. All values fall to very small amounts by the
446 spring following the eruption and return to background levels within a year after the eruption.

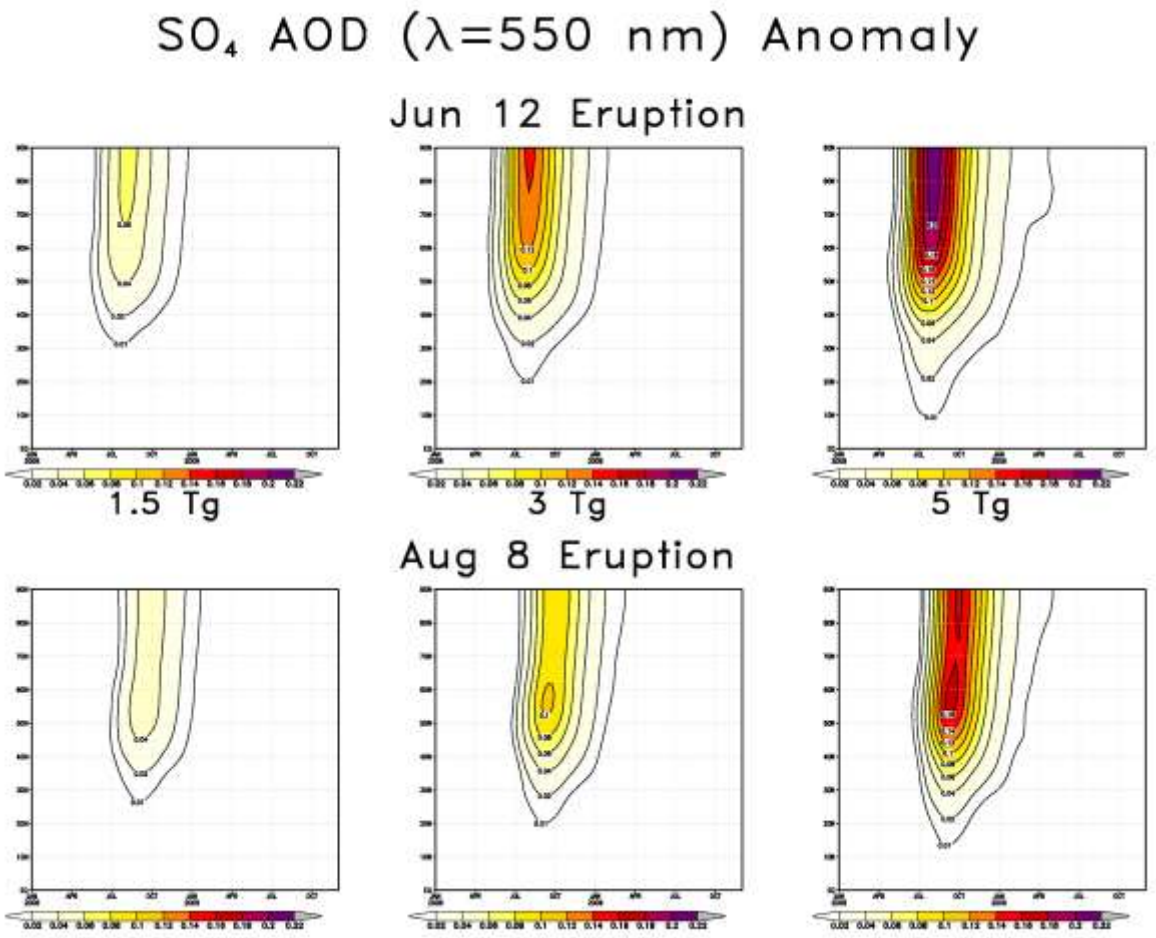

Figure 2. Zonally averaged sulfate aerosol optical depth (mid-visible, λ=550 nm) for all six ensembles. All ensembles pictured are averages of 20 model runs.

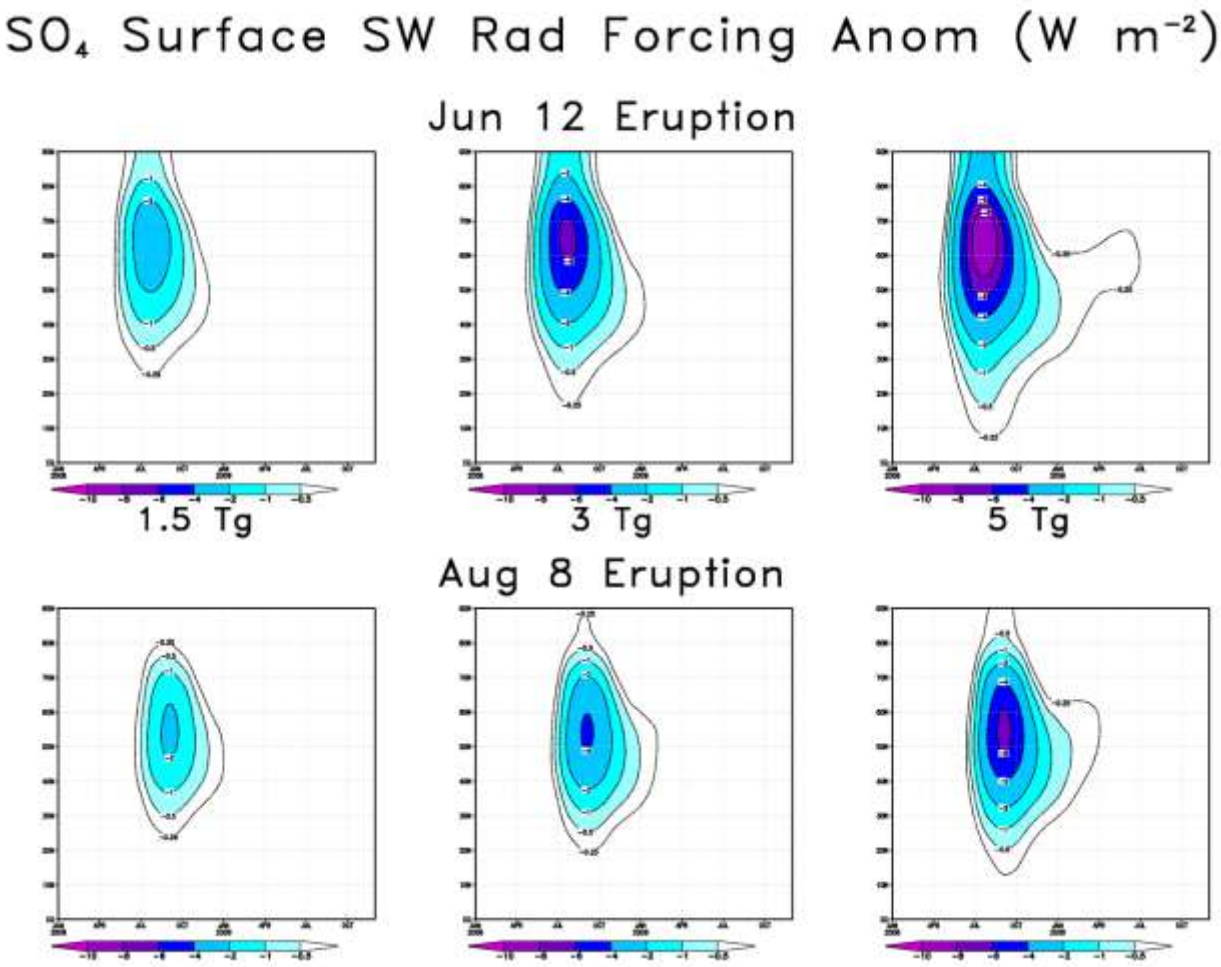

Figure 3. Zonally averaged surface shortwave radiative forcing (W m^{-2}) due to sulfate aerosols for all six ensembles. All ensembles pictured are averages of 20 model runs.

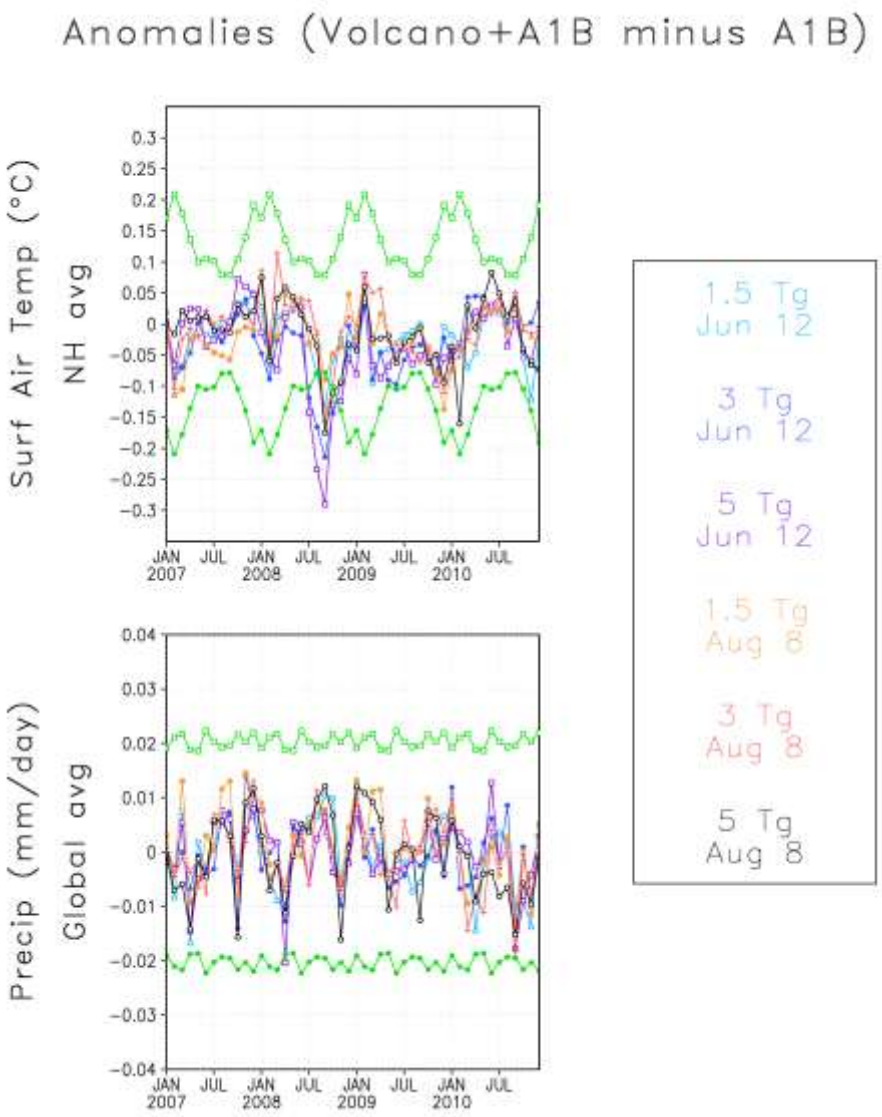

Figure 4. Line graphs of surface air temperature and precipitation anomalies due to the volcanic eruptions. Surface air temperature is averaged over the Northern Hemisphere to amplify changes in temperature over Northern Hemisphere continents, and precipitation is globally averaged. All ensembles are averages of 20 model runs. The light green lines show the average seasonal cycle of the standard deviation from zero anomaly of the control runs as an indication of natural variability. Surface air temperature shows a strong anomaly in the late summer and early autumn following the larger eruptions, whereas the August eruptions do not show particularly significant results. No volcanic signal is detectable in the precipitation results.

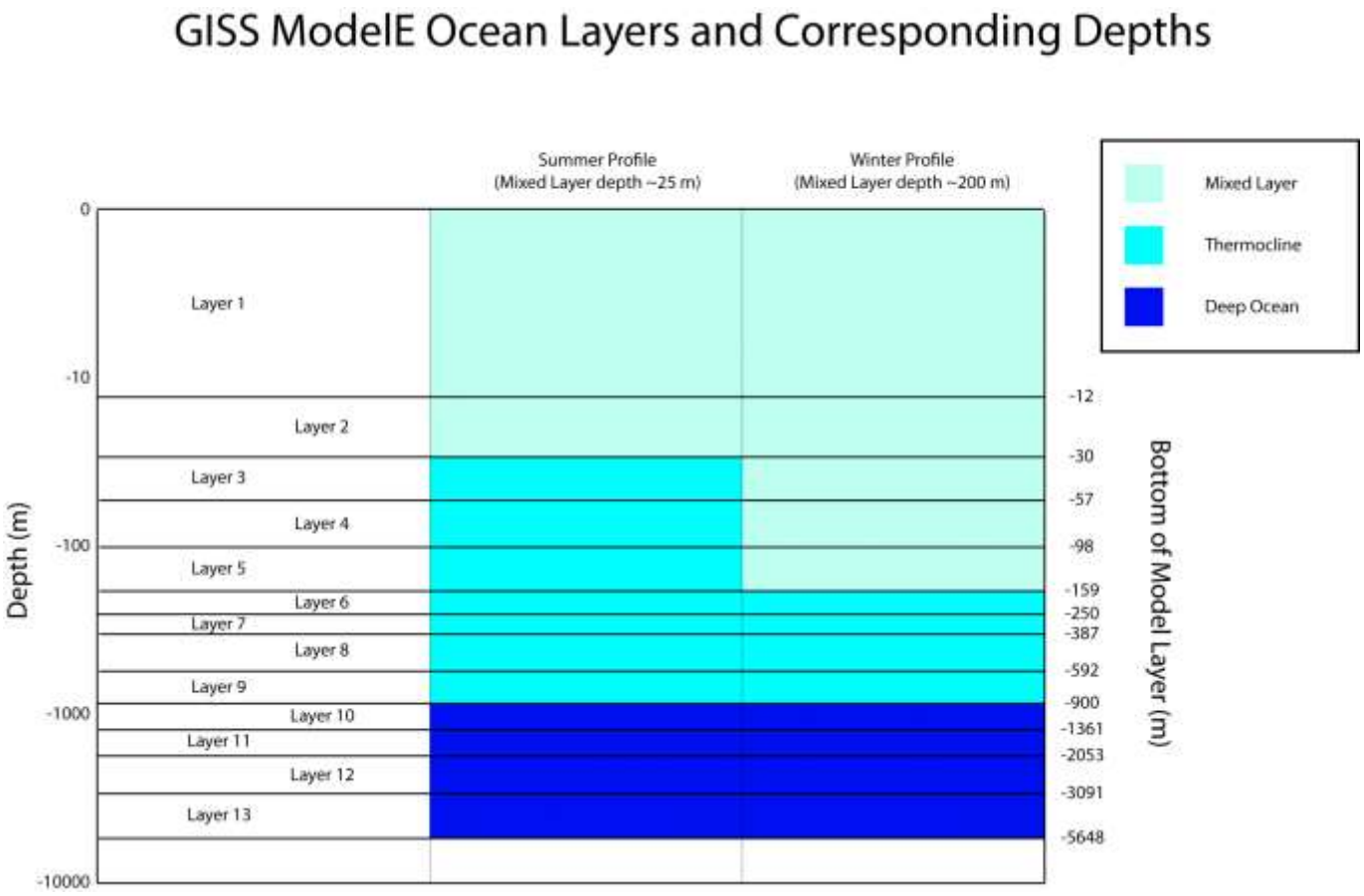

Figure 5. A diagram of the ocean layers in this version of ModelE [*Russell et al.*, 1995]. Model layer thicknesses do not adjust to topography and are either present in their entirety or absent. Determination of the ocean layer by depth follows guidelines in *de Boyer Montégut et al.* [2004], using a thermocline depth range of 25-1000 m in the summer and 200-1000 m in the winter [*Stewart*, 2007].

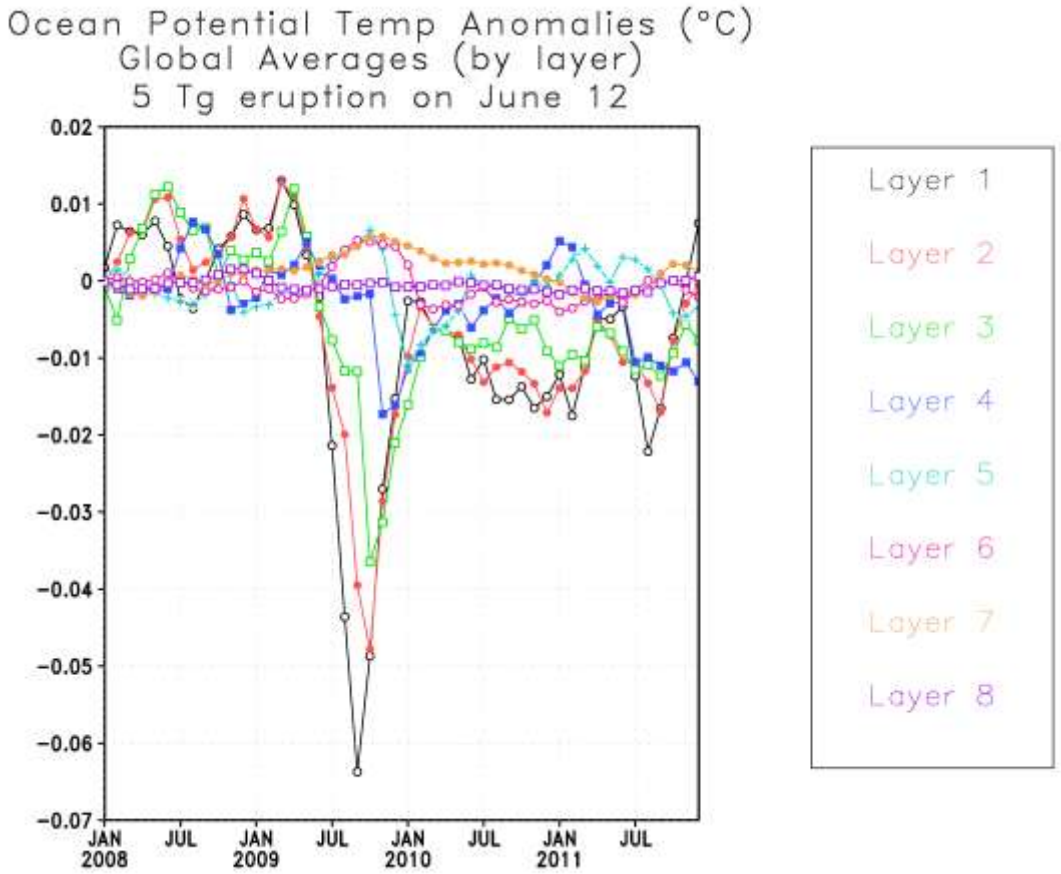

Figure 6. Global average of ocean potential temperature for the top 8 layers (out of 13) in the model. Thicknesses and depths of the layers are given in Figure 5. Layers 1-3 constitute the mixed layer at the time of the eruption, and layers 4-9 constitute the thermocline. All lines shown are for the 5 Tg eruption on June 12 and represent an average of 20 model runs.

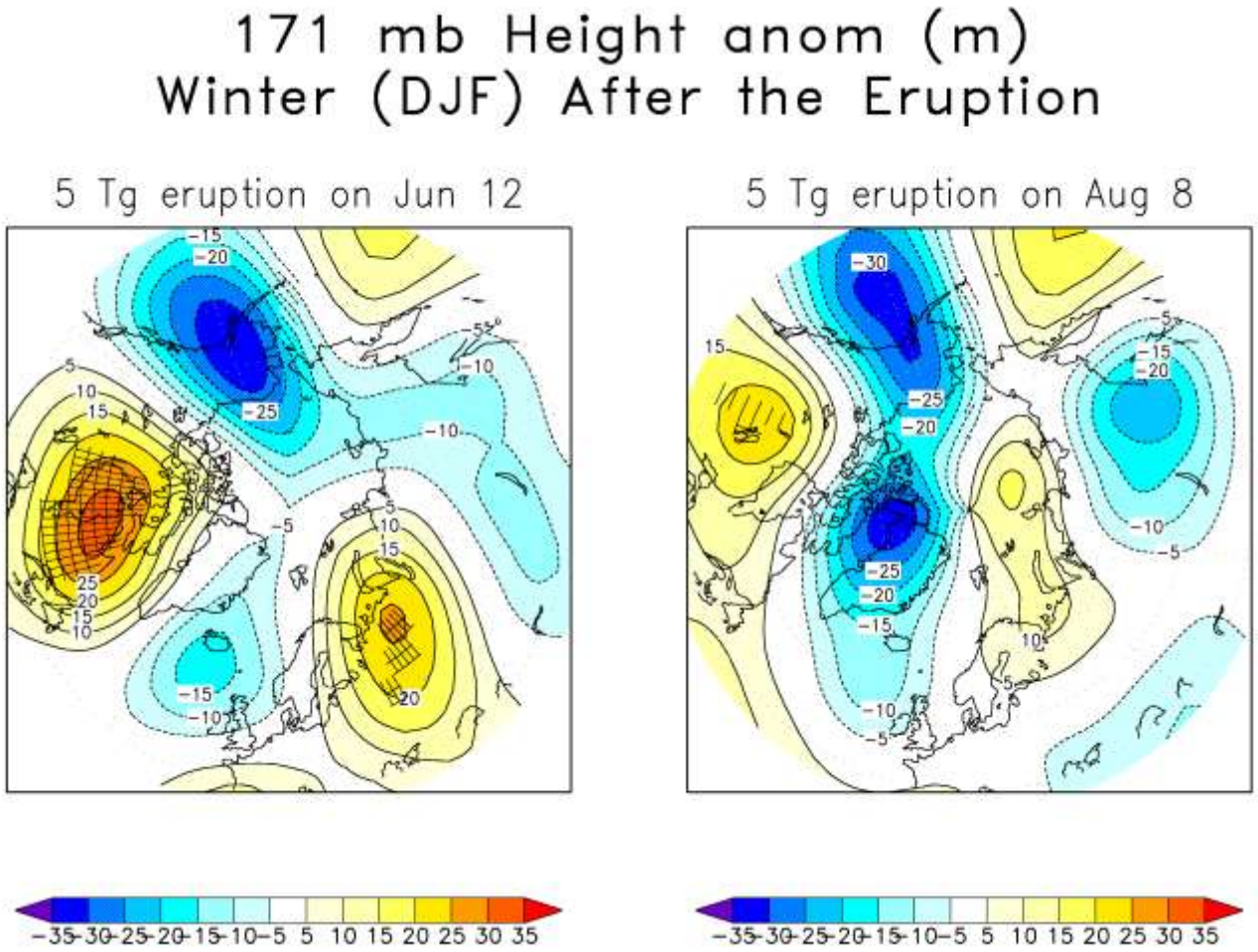

475

476

477 **Figure 7.** A comparison of lower stratospheric (171 mb) height anomalies for the 5 Tg eruptions on June 12 and August 8. Both

478 ensembles are averages of 20 model runs. Statistical significance at the 95% confidence level is denoted by black hatching.

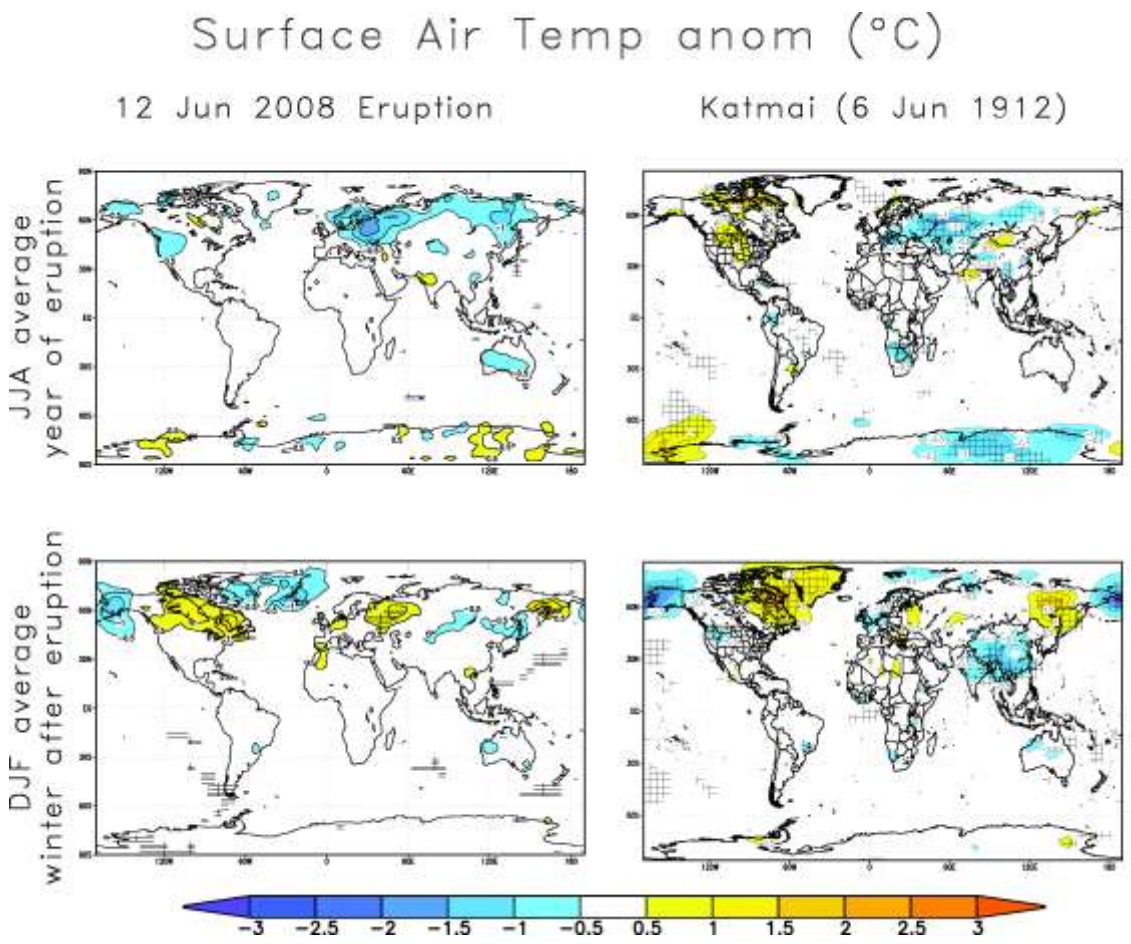

Figure 8. A comparison between simulations of the 5 Tg eruption on June 12, 2008 and simulations of Katmai from *Oman et al.* [2005]. The two right panels are reproductions of figures 7a and 10a from *Oman et al.* [2005]. Statistical significance at the 95% confidence level is denoted by black hatching.